Electrospun Poly(ϵ-caprolactone) Microfiber and Multilayer Nanofiber/Microfiber Scaffolds: Characterization of Scaffolds and Measurement of Cellular Infiltration

Quynh P. Pham,† Upma Sharma,† and Antonios G. Mikos*

Department of Bioengineering, Rice University, MS-142, P.O. Box 1892, Houston, Texas 77251-1892

Received July 13, 2006; Revised Manuscript Received August 9, 2006

The physical and spatial architectural geometries of electrospun scaffolds are important to their application in tissue engineering strategies. In this work, poly(ϵ-caprolactone) microfiber scaffolds with average fiber diameters ranging from 2 to 10 μm were individually electrospun to determine the parameters required for reproducibly fabricating scaffolds. As fiber diameter increased, the average pore size of the scaffolds, as measured by mercury porosimetry, increased (values ranging from 20 to 45 μm), while a constant porosity was observed. To capitalize on both the larger pore sizes of the microfiber layers and the nanoscale dimensions of the nanofiber layers, layered scaffolds were fabricated by sequential electrospinning. These scaffolds consisted of alternating layers of poly(ϵ-caprolactone) microfibers and poly(ϵ-caprolactone) nanofibers. By electrospinning the nanofiber layers for different lengths of time, the thickness of the nanofiber layers could be modulated. Bilayered constructs consisting of microfiber scaffolds with varying thicknesses of nanofibers on top were generated and evaluated for their potential to affect rat marrow stromal cell attachment, spreading, and infiltration. Cell attachment after 24 h did not increase with increasing number of nanofibers, but the presence of nanofibers enhanced cell spreading as evidenced by stronger F-actin staining. Additionally, increasing the thickness of the nanofiber layer reduced the infiltration of cells into the scaffolds under both static and flow perfusion culture for the specific conditions tested. The scaffold design presented in this study allows for cellular infiltration into the scaffolds while at the same time providing nanofibers as a physical mimicry of extracellular matrix.

Introduction

Three-dimensional, porous polymer scaffolds are common in many tissue engineering strategies. A wide array of architectural configurations and geometries can be created using scaffold fabrication technologies such as rapid prototyping, melt extrusion, salt leaching, emulsion templating, phase separation, and electrospinning.[1−7] Electrospinning is a process that can generate fiber mesh scaffolds with high porosities, large surface area-to-volume ratios, and variable fiber diameters.[8,9] These features, along with the versatility and simplicity of the system, make electrospinning an attractive tool for the production of scaffolds.

The principle and theory behind electrospinning has been described in detail in the literature.[10−12] By modulating a combination of solution and processing variables (e.g., the polymer solution concentration, flow rate, collector distance, and applied voltage), fibers with diameters up to 10 μm can be produced.[13] Fiber diameter can have an effect on a variety of scaffold properties, such as porosity, pore size, and surface area.[14,15] These properties, in turn, are important in determining the functionality of scaffolds in tissue engineering applications. The pore size and porosity are critical features of a scaffold that affect cell attachment, proliferation, migration, and/or differentiation.[16−19] Surface topography and structural size-scale are additional parameters that have been shown to affect the orientation and biological function of cells.[20]

The complexity of cell behavior leads to challenges in the design and fabrication of ideal scaffolds for tissue engineering applications. For example, the optimal pore size for cell attachment, proliferation, and migration is not constant across cell types but varies from 5 to 500 μm.[21] A scaffold possessing two or more pore size distributions could facilitate the culture of several cell types to produce multiple interfaces on a single scaffold.[16] Additionally, a scaffold consisting of a gradient in fiber diameter (and thus pore size) has been suggested as a useful model for zonal cartilage tissue engineering.[22] Scaffolds containing gradients in pore size and porosity have also been investigated as bone substitute materials that would allow vascularization and direct osteogenesis on one side while promoting osteochondral ossification on the other.[16,23]

The primary focus in electrospinning has been on the production of nanofibers due to their resemblance scale-wise to native extracellular matrix (ECM).[24] Polymer meshes comprised of fibers with diameters as low as tens of nanometers, and exhibiting porosities as high as 90% and pore sizes as low as 100 nm, have been reported.[24−27] Cells seeded onto nanofiber matrixes tend to spread, attaching at multiple focal points, and in some cases extend filopodia along the length of the fiber.[28,29] Several studies suggest the ability of attached cells to push against nanofibers and migrate into the nanofiber matrix;[28,30,31] however, culture of cells on nanofiber matrixes also results in a monolayer of cells and ECM, thus limiting their potential for 3D tissue engineering applications.[32,33] It has been suggested that smaller fibers can inhibit cellular infiltration.[29] The reduced cellular infiltration into the depths of the scaffold has been attributed to the pore diameters being smaller than that of a cell.[26] For cell migration or infiltration to occur, the pore size of a scaffold should at least be the size of a cell;[32] a value of 10 μm has been suggested as necessary for cellular infiltration.[34]

* Corresponding author. Phone: (713) 348-5355. Fax: (713) 348-4244. E-mail: mikos@rice.edu.

† Authors contributed equally to this work.

10.1021/bm060680j CCC: $33.50
Published on Web 09/23/2006

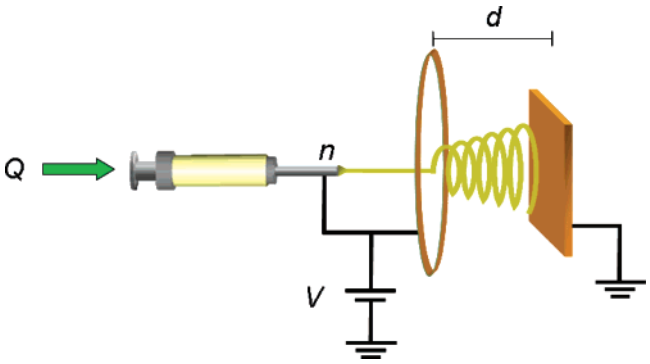

Figure 1. Schematic representation of the electrospinning setup. The flow rate (Q), distance (d), applied voltage (V), needle gauge (n), and polymer solution properties could all be varied to affect the properties of the resulting fibers.

Although there has been much research related to nanofiber applications, there has been little reported on the electrospinning of electrospun microfiber scaffolds. Although microfiber scaffolds are not on the same size scale as ECM components, they could be potentially advantageous because they are comprised of larger pores as compared to nanofiber scaffolds. These larger pore sizes scaffolds could allow or facilitate cellular infiltration and/or diffusion of nutrients during in vitro culture.[35] In a study by Badami et al., MC3T3-E1 osteoprogenitor cells exhibited more proliferation on 2.1 μm fibers as compared to 0.14 μm fibers, suggesting that cells on the microfiber scaffolds were able to penetrate into the scaffold and continue proliferating.[29]

In this study, we investigated the electrospinning of poly(ϵ-caprolactone) (PCL) microfiber scaffolds. PCL is a biocompatible, biodegradable polymer that has been successfully electrospun; furthermore, it has been shown to be capable of supporting a wide variety of cell types, including marrow stromal cells (MSCs).[36] Electrospun scaffolds were characterized in terms of fiber diameter (measured by electron microscopy), pore size (measured by mercury porosimetry), and porosity (measured by mercury porosimetry, liquid intrusion, and gravimetry). The ability to generate a wide range of fiber diameters (5 nm to 10 μm) by electrospinning allows for the possibility of designing fiber scaffolds with multimodal characteristics to regulate the biological function of cells. Therefore, in addition to the microfiber scaffolds, we have utilized a multilayering technique to construct a bimodal scaffold consisting of alternating layers of micro- and nanofibers. Using this strategy, the inherent advantages of both nanofibers and microfibers can be realized in a single scaffold. Bilayered scaffolds consisting of a top nanofiber layer and a bottom microfiber layer were used as model systems to investigate the effect that nanofibers have on rat MSC attachment, spreading, and migration; static and flow perfusion culture conditions were considered.

Methods

Electrospinning Apparatus. Nonwoven electrospun scaffolds were electrospun using the schematic shown in Figure 1. The setup consists of a syringe pump (Cole Parmer, Vernon Hills, IL), power supply (Gamma High Voltage Research, Ormond Beach, FL), and a square grounded copper plate (11 × 11 × 0.3 cm). A 10 mL syringe was filled with the appropriate polymer solution; the syringe was then fitted with a blunt needle tip (Brico Medical Supplies, Inc, Metuchen, NJ). A 19 cm diameter copper wire (18 gauge) ring was placed 6 cm in front of the tip of the capillary tip. The positive lead from the power supply was split and attached to both the needle and the copper ring. During electrospinning, the fibers were collected onto a glass plate (0.22 cm thick) placed directly in front of the copper plate. After electrospinning, electrospun sheets were dried overnight in a desiccator. Samples (8 mm diameter discs) were cut from the dried sheets using an arch punch (C. S. Osborne & Co., Harrison, NJ).

Electrospinning. PCL (MW = 80 000, Sigma, St. Louis, MO) was used for electrospinning. A series of PCL polymer solutions (8−15 wt %) were prepared in chloroform:methanol ratios of 5:1, 6:1, or 7:1 (by vol) for the electrospinning of microfibers. Table 1 shows the solution and processing variables used to electrospin the different microfiber scaffolds. Q is the flow rate, d is the collector distance (from ring to collector), n is the needle gauge (length = 1.5 in.), and V is the applied voltage. For electrospinning 2 μm fibers, a parallel plate configuration[11] was used in addition to the ring. PCL nanofibers were obtained by electrospinning an 11 wt % PCL solution in a 1:1 (by vol) ratio of chloroform:*N*,*N*-dimethylformamide at the following conditions: d = 15 cm, V = 14 kV, Q = 0.8 mL/h, and n = 25.

Scaffold Morphology. Electrospun scaffolds were sputter-coated with gold for 1 min and observed with an FEI-XL 30 environmental scanning electron microscope (Mawah, NJ) at an accelerating voltage of 20 kV. For quantification of fiber diameter, measurements were made on the first five fibers that intersected a line drawn across the middle of an image (at 2000× magnification). Images from five random locations (selected blindly at 100× magnification) at the top and bottom of the scaffold were used for a total of 50 measurements.

Bilayered scaffolds consisting of a top nanofiber layer (600 nm) and a bottom 5 μm microfiber layer were electrospun by sequentially electrospinning under the appropriate conditions listed in Table 1. The nanofiber density for different nanofiber electrospin times was characterized by counting the number of fibers that intersected a line drawn across the middle of the image. The percent coverage of nanofibers was taken as the number of nanofibers divided by the total number of fibers (microfiber and nanofibers) that intersected the line. To ensure uniformity and reproducibility of each condition, five different polymer sheets were electrospun, and five samples were taken from each sheet (top, middle, bottom, left, and right of the sheet). From each sample, three measurements were made (at three different magnifications 2000×, 2500×, and 3000×) for a total of 75 counts per condition. The frequency of counts (expressed as a percentage) was graphed as a function of the percent coverage of nanofibers (grouped in 10% bins). For example, a frequency of 20% for the 30% bin would indicate that 15 of the areas examined displayed between 20% and 30% coverage by nanofibers. Herein, these bilayered scaffolds are referred to by the nanofiber electrospin time (e.g., a 30 s scaffold refers to a 5 μm microfiber layer with a nanofiber layer on top produced by electrospinning nanofibers for 30 s).

Cross-sectional images of multilayered scaffolds were obtained by submerging the scaffolds in liquid nitrogen and cutting with titanium scissors. The samples were prepared for SEM as described above. To enhance the contrast between nanofibers and microfibers in the SEM images, nanofibers and microfibers (based on measurement) were manually false-colored using GNU Image Manipulation Program software (available on the Internet under a General Public License).

Mercury Porosimetry. Pore sizes of scaffolds comprised of microfibers were measured by using mercury porosimetry (Autoscan 500, Quantachrome Instruments, Boynton Beach, FL). Scaffolds (≥1 mm in thickness) were weighed and placed into the sample chamber, and the void space in the chamber was filled with mercury (initial pressure ≈ 0.6 psi). The pressure was then increased at a rate of 0.01 psi/s until a total pressure of 50 psi was reached. The range of pore diameters, d_p, that could be measured using this approach could be calculated using the Washburn equation:

$$d_p = \frac{-4\gamma \cos\theta}{P}$$

where γ is the surface tension of mercury, θ is the contact angle between the mercury and the scaffold, and P is the pressure. As reported in the literature,[37] a contact angle of 140° between PCL and mercury in air

Table 1. Electrospinning Processing Conditions for PCL Scaffolds

targeted fiber diameter (μm)	PCL concentration (wt %)	solvent mixture (by vol)	collector distance (cm)	voltage (kV)	flow rate (mL/h)	needle gauge
0.6	11	1:1[a]	15	14	0.8	25
2	8	7:1	18.5	27	3.5	22
3	9	6:1	15	19	4.5	18
4	10	7:1	16.5	20	8	18
5	12	5:1	19.5	22	8	18
6	13	5:1	23.5	22.5	8	18
7	14	5:1	28	24	8	16
8	14	5:1	33	27	10	16
10	14	5:1	33	25.5	18	16

[a] Solvent mixture is chloroform:*N*,*N*-dimethylformamide; all other scaffolds were made using chloroform:methanol at the specified ratio (by volume).

was used. Therefore, the pressure range of 0.6−50 psi corresponds to pores ranging from 4 to 360 μm in diameter. The volume versus pressure data were converted to pore size, porosity, and surface area by using software supplied by the vendor (Quantachrome Instruments AUTOSCAN, ver. 3.00). Measurements were made on three samples of each scaffold type.

Porosity. The porosity of the microfiber scaffolds was also measured using gravimetry and liquid intrusion methods. Scaffolds ($n = 3$) were weighed prior to immersion in ethanol (liquid intrusion). A brief vacuum was applied for 10 min, and the scaffolds were left overnight on a shaker table to allow diffusion of ethanol into the void volume. The scaffolds were taken out, blotted with a Kimwipe, and reweighed. The porosity was calculated by dividing the volume of intruded ethanol (as determined by the change in mass due to intrusion and the density of ethanol, 0.789 g/mL) by the total volume after intrusion (i.e., volume of the intruded ethanol combined with the volume of the PCL fibers determined from the initial mass of the PCL scaffold and the density of PCL, 1.145 g/mL).

For gravimetric measurements, the thicknesses of the scaffolds were measured using micro-calipers. Using the measurement of the thickness and knowing the diameter (8 mm) of the scaffolds, the volume of the scaffold could be determined. The mass of the scaffold was also measured allowing for determination of the apparent density of the scaffold, ρ_{scaffold}. The porosity, ϵ, was then calculated according to the equation,

$$\epsilon = 1 - \frac{\rho_{\text{scaffold}}}{\rho_{\text{material}}}$$

where ρ_{material} is the density of PCL.[38]

Scaffold Preparation. Preparation of the scaffolds for cell seeding consisted of sterilization, prewetting, and press-fitting phases. Scaffolds were first sterilized with ethylene oxide gas for 14 h. They were then transferred to a centrifuge tube and underwent a gradient ethanol series to 70% and were left overnight. Centrifugation was performed to ensure complete wetting. The ethanol was then exchanged with three rinses of phosphate buffered saline and then with culture media and left in the incubator overnight. Prior to seeding, the scaffolds were press-fit into cassettes (designed for static and flow perfusion culture) and placed in a 6-well plate for seeding, as previously described.[13]

Cell Culture Experimental Design. To investigate the applicability of the microfiber and micro-/nanofiber layered scaffolds, we quantified cell attachment, spreading, and infiltration on 0 (microfiber scaffold with no nanofiber layer on top), 30, 90, and 300 s scaffolds. MSCs from male Fischer 344 rats (Harlan, Indianapolis, IN) were isolated and stored as previously described.[13] The prepared scaffolds were seeded with 250 000 MSCs in 200 μL of complete osteogenic media. Quantification of cellular attachment was performed on 4 scaffolds from each group at 2 and 24 h post-seeding. An additional scaffold from each group at both time points was used to stain F-actin to visualize cell spreading.

Twelve constructs from each group were also prepared for culture under static and dynamic conditions for determination of cellular infiltration. Scaffolds (die-punched into disks with dimensions of 8 mm in diameter and thicknesses between 1 and 1.2 mm) were prepared for seeding as described above. After the 2 h attachment period, the wells of the tissue culture plate were filled with 9 mL of complete media. Twenty-four hours after seeding, six cassettes from each group containing the cell-seeded scaffolds were transferred to a flow perfusion bioreactor system driven by a peristaltic pump operating at a flow rate of 1 mL/min as described previously.[13] The constructs were cultured in complete media under static or flow perfusion culture for 12 d with media changes every 48 h. At the end of the culture period, 4 constructs were used for histological analysis and 1 for scanning electron microscopy.

Cell Attachment and Spreading. The cellularity of the constructs was determined using a fluorometric double-stranded DNA quantification kit.[13] To extract the DNA, constructs were first digested in a proteinase K solution as previously described.[13] To do so, samples were transferred to 1.25 mL of Tris/EDTA buffer (6.055 mg/mL Tris-(hydroxymethyl aminomethane), 0.372 mg/mL EDTA, pH 7.6 adjusted by HCl). Samples were digested at 56 °C for 16 h after adding 250 μL of a proteinase K solution (1 mg/mL proteinase K, 10 μg/mL pepstatin A, and 185 μg/mL iodoacetamide in Tris/EDTA buffer). To ensure complete extraction, the constructs were then subjected to three repetitions of a freeze/thaw cycle (10 min at −80 °C, 10 min at 37 °C) followed by 20 min of sonication. The supernatant of the solution was used to measure the cellularity of the scaffolds by measuring double-stranded DNA using the PicoGreen assay (Molecular Probes, Eugene, OR) according to the manufacturer's instructions. The results were expressed as cells per construct using a standard DNA curve created with double-stranded DNA standards and DNA extracted from known numbers of MSCs.

After 2 and 24 h post-seeding, scaffolds were removed from the cassettes and stained for F-actin with rhodamine phalloidin (Molecular Probes, Carlsbad, CA) according to the manufacturer's specifications. Briefly, the scaffolds were rinsed in PBS and fixed in 10% neutral buffered formalin (Sigma, St. Louis, MO) for 10 min. The scaffolds were then rinsed in PBS and washed with 0.1% Triton X-100 (Fisher Scientific, Pittsburgh, PA) in PBS for 5 min to permeabilize the cell membranes. After being rinsed in PBS, the scaffolds were incubated in 1% bovine serum albumin (Sigma, St. Louis, MO) in PBS for 20 min to reduce nonspecific background staining. Finally, the scaffolds were stained with rhodamine phalloidin at the concentration recommended by the manufacturer for an additional 20 min before visualization. Images were recorded using a laser scanning confocal microscope (Zeiss LSM 510 Axiovert, Carl Zeiss, Germany) under a He/Ne laser (ex/em: 543/565 nm).

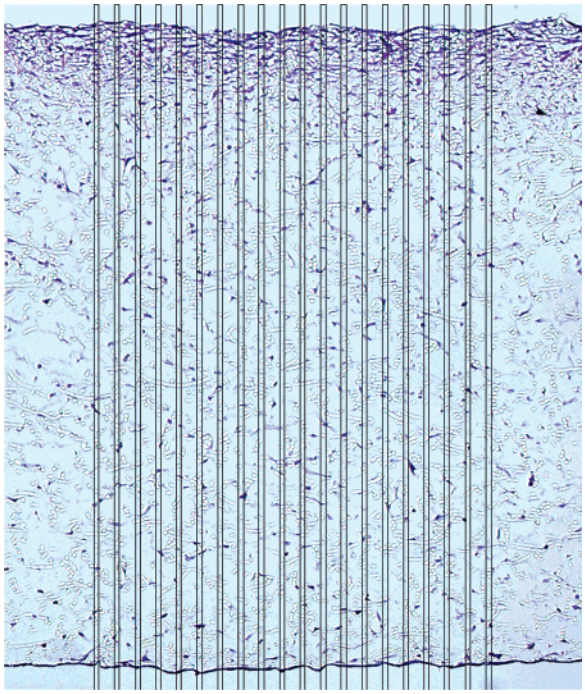

Figure 2. Representative light micrograph (10× magnification) of a cross-section of a PCL microfiber scaffold after staining with hematoxylin and eosin and cryosectioning. The grid was overlaid to allow for quantification of infiltration depth. Lines on the grid are separated by 30 μm and are 10 μm wide.

Histology. For histological analysis, the scaffolds were processed on the basis of a protocol adapted from Holy and Yakubovich.[39] After the culture period, the scaffolds were harvested from the culture cassettes and placed in 10% neutral buffered formalin for further processing. All scaffolds were rinsed in ddH_2O and placed in Weigert's iron hematoxylin (Sigma, St. Louis, MO) for 5 min under vacuum to ensure distribution of the stain throughout the scaffold; they remained in the hematoxylin for an additional 13 min and were then rinsed with ddH_2O. After being rinsed in 100% ethanol, samples were stained with alcoholic eosin Y (Sigma, St. Louis, MO) in a similar manner. The scaffolds were then immersed in 70% ethanol until all residual eosin was removed and embedded in Histo-Prep freezing medium (Fisher Scientific, Pittsburgh, PA). Frozen sections of 5 μm thickness were obtained using a cryostat (HM500, Microm, Walldorf, Germany) operating at −23 °C and mounted onto Superfrost Plus glass slides (Fisher Scientific, Pittsburgh, PA). The slides were allowed to dry overnight at 37 °C and mounted with Permount (Fisher Scientific, Pittsburgh, PA). Images were obtained with a light microscope (Eclipse E600; Nikon, Melville, NY) and attached video camera (3CCD Color Video Camera DXC-950P; Sony, Park Ridge, NJ).

To quantify these results, a grid was overlaid on the obtained images. This grid consisted of 20 10-μm thick "lines"; these lines were spaced evenly (30 μm apart) (Figure 2). To measure the cell infiltration, each of the lines was examined. The distance between the cell that was most penetrated and the top of the scaffold at that line was measured, as well as the thickness of the scaffold at that line. (For example, the sample image (Figure 2) demonstrated 100% infiltration.) Each image yielded 20 measurements of infiltration depth. For each scaffold, sections that were spaced by at least 500 μm were examined using this procedure; 4 sections were examined per scaffold. For each experimental group (nanofiber electrospin times of 0, 30, 90, and 300 s), 4 scaffolds were evaluated using this procedure. Therefore, each experimental group had the infiltration depth analyzed using 320 different lines.

Statistical Methods. Fiber diameter and porosity results are expressed as means ± standard deviation. Statistical differences between the fiber diameter size at the top and bottom of the microfiber scaffolds were determined by performing a Student's *t*-test (confidence interval of 99%). A single factor analysis of variance was performed to determine whether a significant difference existed between the porosity values measured using the different techniques for each targeted fiber diameter. Multiple pairwise comparisons were made using the Tukey procedure at a significance level of 99%. Cell infiltration distance and attachment results are expressed as means ± standard deviation. A full two-factor analysis of variance with random-effect, nested factors was performed for both to determine any significance prior to making multiple pairwise comparisons using the Tukey procedure at a significance level of 99%.

Results and Discussion

In this study, we explored the electrospinning of PCL micro- and nanofibers to generate 3D scaffolds for tissue engineering applications. Specifically, the first part of this work focused on the characterization of microfiber scaffolds with respect to fiber diameter, pore size, porosity, and surface area. Additionally, results were compared to those obtained using a theoretical model. In the second part of this study, we capitalized on the versatility of electrospinning to fabricate (through multilayering electrospinning) scaffolds composed of alternating layers of micro- and nanofibers. In particular, we wanted to determine the effect of duration of electrospinning on the percent coverage of nanofibers on top of an existing microfiber layer. Finally, we illustrated the potential use of these scaffolds by evaluating cell attachment, spreading, and infiltration on bilayered scaffolds of nano- and microfibers.

Electrospinning and Characterization of Microfiber Scaffolds. The electrospinning setup used in this study is a variation on the dual electrode setup.[40] We found that this arrangement caused the convergence of collected fibers into a confined circular space, helping to decrease the necessary time to produce three-dimensional scaffolds greater than 1 mm in thickness. Scaffolds with thicknesses near 1 mm have been considered before for tissue engineering applications as described previously.[13] Using the electrospinning system, conditions for reproducibly fabricating scaffolds with different diameters were investigated. A common solvent used for electrospinning PCL is a 3:1 (by vol) chloroform:methanol mixture;[11,41] however, we observed that, during the course of electrospinning, the Taylor cone became unstable and would occasionally drip, leading to irregular fiber formation. By increasing the chloroform:methanol ratio to 5:1 or higher, a stable Taylor cone was produced, allowing for prolonged electrospinning of microfibers.

Because of the interdependence of the Taylor cone stability and the electrospinning variables (e.g., flow rate, applied voltage, collector distance), this study focused on obtaining the conditions necessary to generate the targeted fiber diameters rather than determining the effect of individual variables on fiber diameter. For example, an increase in collector distance often had to be complemented with an increase in applied voltage to keep the Taylor cone stable over the course of electrospinning a three-dimensional scaffold. In general, increasing the flow rate and the concentration of PCL required a larger applied electric field and longer collector distance yielding increased fiber diameter (Table 1). As shown in Table 2, by varying the electrospinning solution and processing conditions, scaffolds with fiber diameters ranging from approximately 2 to 10 μm were generated in a reproducible manner. (In this table, the "targeted fiber diameter" refers to the average fiber diameter of the scaffold, rounded to the nearest integer. For example, the scaffold with an average fiber diameter on top and bottom of 2.12 ± 0.45 and 2.34 ± 0.29 μm, respectively, is referred to

Table 2. Average Fiber Diameters from the Top and Bottom of Microfiber PCL Scaffolds Fabricated Using the Conditions Described in Table 1[a]

targeted fiber diameter (μm)	actual fiber diameter, top (μm)	actual fiber diameter, bottom (μm)
2	2.12 ± 0.45	2.34 ± 0.29
3	3.18 ± 0.35	3.05 ± 0.39
4	4.01 ± 0.49	3.95 ± 0.51
5	4.86 ± 0.56	4.96 ± 0.46
6	6.37 ± 0.55	6.13 ± 0.37
7	6.90 ± 0.84	6.78 ± 0.85
8	7.94 ± 0.37*	7.30 ± 0.46*
10	10.8 ± 0.81*	9.57 ± 0.72*

[a] Measurements represent the mean and standard deviations of 25 fiber diameters on the top and bottom sides of the scaffolds. A "*" indicates a statistically significant difference ($p < 0.01$) between the top and bottom of the scaffolds.

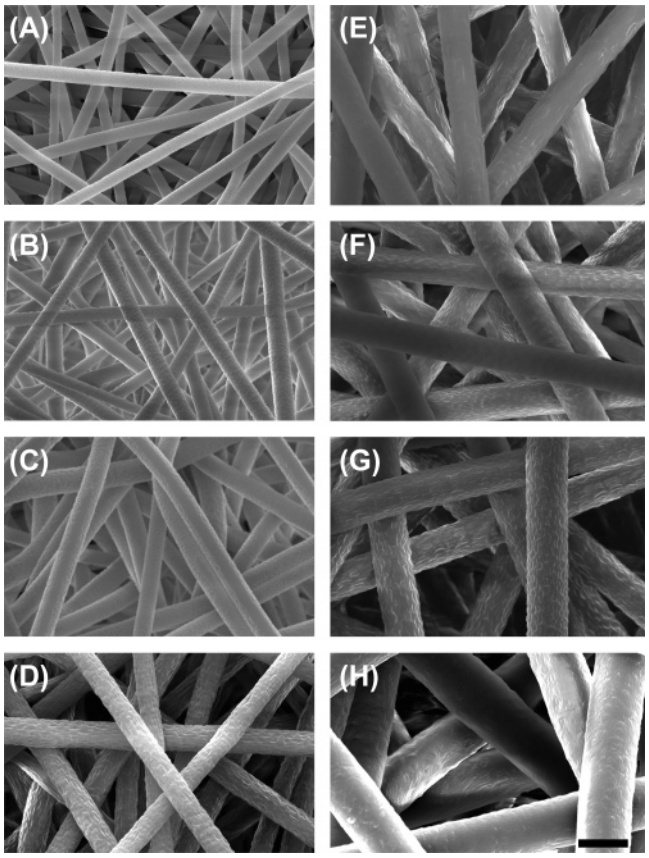

Figure 3. Scanning electron micrographs of electrospun microfibers consisting of (A) 2 μm, (B) 3 μm, (C) 4 μm, (D) 5 μm, (E) 6 μm, (F) 7 μm, (G) 8 μm, and (H) 10 μm fiber diameters. The scale bar shown applies to all images and is equal to 10 μm.

as having a targeted fiber diameter of 2 μm.) Addition of the parallel plate to the ring setup increased the uniformity of 2 μm fibers, but was unnecessary for larger fiber diameters. The top sides of these microfiber scaffolds are shown in Figure 3. Statistically significant differences in the fiber diameters on the top and bottom sides of the scaffolds were observed for the scaffolds comprised of 8 and 10 μm fibers, indicating that it became more difficult to control fiber diameter at larger diameters. Investigation into this phenomenon revealed that the fiber diameters gradually increased for the first 5 min and then reached a plateau (data not shown).

Because pore size and porosity are critical features of a scaffold that influence the behavior of seeded cells, microfiber

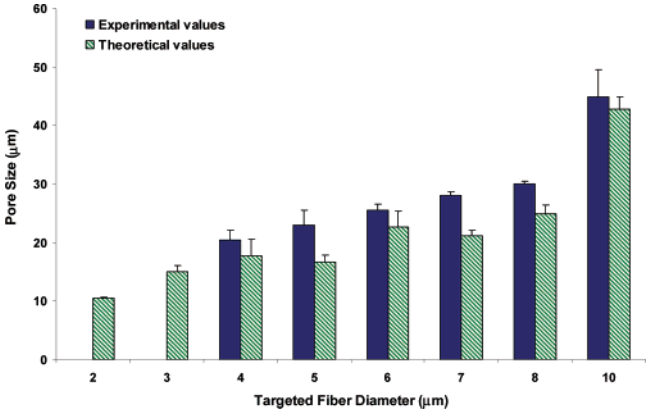

Figure 4. The pore size of microfiber scaffolds plotted as a function of fiber diameter. Experimental measurements were performed by mercury porosimetry. Theoretical values were calculated using porosity measurements obtained by averaging measurements from mercury porosimetry, liquid intrusion, and gravimetry. The experimental data represent the average of three samples with the error bars representing the standard deviations. Error bars on the theoretically predicted pore sizes are computed using the standard deviation of the input porosities and fiber diameters.

scaffolds were characterized with respect to these properties. Pore sizes were experimentally determined using mercury porosimetry and varied from approximately 20 to 45 μm for scaffolds comprised of 4−10 μm fiber diameters, respectively (Figure 4). The pore size of scaffolds made up of 2 and 3 μm fibers could not be determined because at the maximum pressure (50 psi) of the mercury porosimeter the intrusion volume had not reached a plateau.[42] Using pressures greater than 50 psi would likely result in collapse and compression of the scaffold.[43] Therefore, for electrospun scaffolds comprised of fibers with diameters less than 3 μm, mercury porosimetry may not be a suitable technique for measurement of the pore size.

Porosities of the microfiber scaffolds were measured using three different techniques: mercury porosimetry, liquid intrusion, and gravimetry. It was expected that the liquid intrusion would yield an overestimation of the porosity of the scaffold due to diffusion of the ethanol into the fibers. Conversely, the mercury porosimetry was expected to underestimate the porosity because pores smaller than 4 μm will not be measured (see Methods). However, there was no statistical difference between the porosities measured by these three techniques (Figure 5). In all methods, the measured porosities were between 84% and 89% regardless of the measurement technique selected.

Comparison of Experimentally Measured and Theoretically Predicted Pore Sizes. To estimate the pore size of electrospun scaffolds, a previously developed theoretical model was applied.[14,44] In this model, an electrospun scaffold was considered to be a collection of randomly placed straight rods. In developing this model, two-dimensional random networks were first considered;[44] the mean pore radius of these two-dimensional networks was computed on the basis of the porosity and mean fiber diameter. To do so, it was assumed that the pore radii of these planes followed a Poisson distribution. The coefficient of variation of the pore radius was taken to be a constant that has been previously calculated for random networks.[14,44] This approach was extended by considering the three-dimensional scaffold as a superposition of n two-dimensional layers. Doing so allowed the average pore radius,

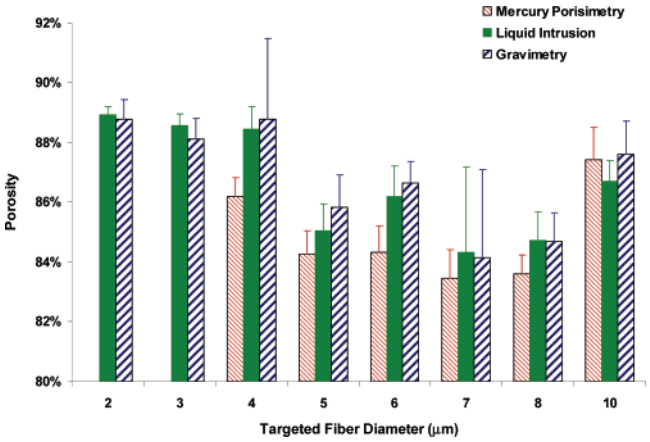

Figure 5. Comparison of the porosities of microfiber scaffolds measured using mercury porosimetry, liquid intrusion, and gravimetry. The data represent means of three samples with the error bars representing the standard deviations. No significant differences were found between the porosities at each fiber diameter using the three measurement techniques ($p < 0.01$).

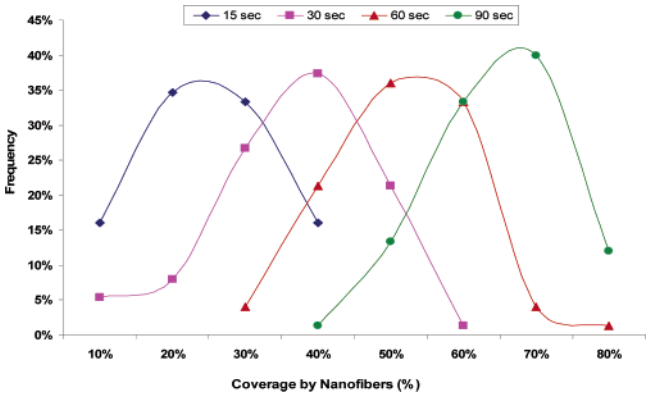

Figure 6. Multilayer scaffolds were characterized in terms of the distribution of the coverage of nanofibers on top of an existing microfiber (5 μm fiber diameter) layer. For each layered scaffold condition, 75 randomly selected points were examined; the data represent the frequency of occurrences of a particular coverage of nanofibers. The percent coverage of nanofibers was grouped into 10% bins (e.g., 30% coverage by nanofibers indicates between 21% and 30% coverage).

$\bar{r}$, to be calculated using the following equation:

$$\bar{r} = \int_0^\infty r \frac{n}{\epsilon}\left(\frac{\Gamma(k,br)}{\Gamma(k)}\right)^{(n/\epsilon)-1} \frac{b^k}{\Gamma(k)} r^{k-1} e^{-br}\, dr$$

where k and b characterize the gamma distribution, Γ, that describes the distribution of pore radii in two dimensions,[14] and ϵ is the porosity.

Using the porosity (as measured by averaging the values obtained from the three techniques mentioned above) and fiber diameter measurements obtained from SEM, the predicted pore sizes of the microfiber scaffolds were calculated using the above equation. (Note: the error bars on the theoretical measurements are based on error in the porosity measurements.) These theoretically predicted values were compared with experimentally measured pore sizes obtained via mercury porosimetry (Figure 4). These results demonstrate that increasing the fiber diameter of the scaffolds yielded an increase in the pore size, as previously demonstrated.[14] For all conditions, the predicted pore size was smaller than those measured experimentally using mercury porosimetry. The differences between all theoretically predicted and experimentally measured pore sizes were less than 1.5-fold.

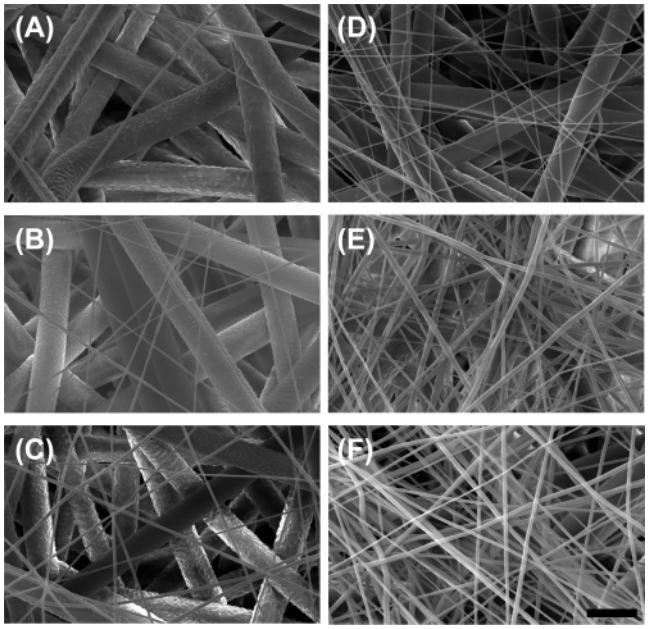

Figure 7. Scanning electron micrographs depicting the effect of different periods of nanofiber electrospinning times on the accumulation of nanofibers on top of an existing microfiber layer (5 μm fiber diameter): (A) 15 s electrospin, (B) 30 s electrospin, (C) 60 s electrospin, (D) 90 s electrospin, (E) 120 s electrospin, and (F) 300 s electrospin. The average fiber diameters are 610 $\pm$ 120 nm and 5 μm for the nano- and microfibers, respectively. The scale bar shown applies to all images and is equal to 10 μm.

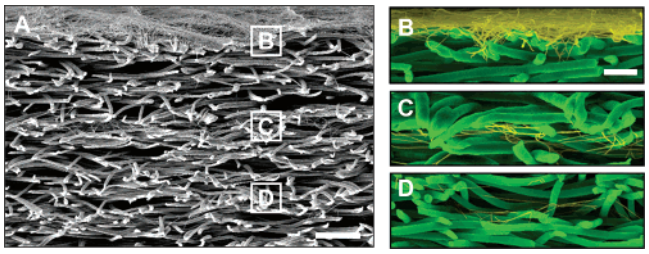

Figure 8. Scanning electron micrographs of cross-sections of layered scaffolds generated by sequential electrospinning. (A) Cross-section illustrating (from top to bottom) a nano-micro-nano-micro-nano-microfiber layered scaffold. The white boxes correspond to the nanofiber layers and their respective magnified images shown to the right. (B) Magnification of the nanolayer electrospun for 5 min. (C) Magnification of the nanolayer electrospun for 90 s. (D) Magnification of the nanolayer electrospun for 30 s. The scale bar shown for (A) is 100 μm, and for (B−D) it is 25 μm. Microfibers are false colored green while nanofibers are false colored yellow to enhance contrast.

Because the pore sizes of scaffolds made up of 2 and 3 μm fibers could not be accurately measured using mercury porosimetry, they were estimated using the theoretical model. For these scaffolds, the porosity was first measured using liquid intrusion and gravimetry. The average porosity (determined by averaging the measurements), along with fiber diameter sizes obtained via SEM, was input into the theoretical model to estimate the pore size. Pore sizes of 10.5 $\pm$ 0.1 and 14.9 $\pm$ 1.0 μm were calculated for the scaffolds comprised of 2 and 3 μm fibers, respectively. These results illustrate the utility of the model: when experimental approaches are not readily available for the characterization of the pore size of electrospun scaffolds, the model can be used to provide an estimate. These estimated values agree well with experimentally measured ones for all conditions tested (4−10 μm fibers). Furthermore, all that is required to estimate the pore sizes with the model is a

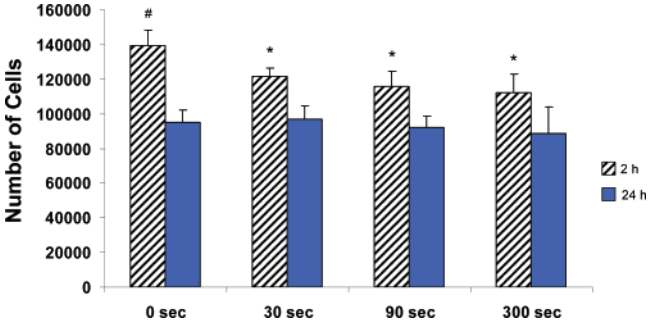

Figure 9. Cell attachment on 0, 30, 90, and 300 s scaffolds at 2 and 24 h post-seeding. The 0, 30, 90, and 300 s scaffolds are bilayered scaffolds consisting of a bottom microfiber layer (5 μm) and a top nanofiber layer (600 nm); the numbers correspond to the time used to spin the nanofiber layer. The data represent means of four samples, with error bars representing the standard deviations. A "*" indicates significance ($p < 0.01$) with respect to the 24 h time point within the group; a "#" indicates significance ($p < 0.01$) against all groups at both time points.

measurement of the porosity and the average fiber diameters of the scaffold.

Fabrication and Characterization of Multilayered Scaffolds. In this work, we fabricated novel scaffolds to combine the beneficial properties of nanofibers and microfibers. To do so, we employed multilayering electrospinning to create scaffolds that included both nano- and microfiber layers. Multilayering electrospinning was demonstrated by Kidoaki et al. in which layered scaffolds were fabricated by sequentially electrospinning different polymers.[45] Rather than changing the polymers, we applied multilayering to electrospin layers of the same polymer but with different morphologies. Specifically, PCL nanofibers of approximately 600 nm were electrospun onto 5 μm PCL fibers to form a bilayered scaffold. By exchanging and alternately electrospinning the two polymer solutions and conditions (see Methods for the solution and processing conditions required to produce micro- and nanolayers), a scaffold with bimodal morphological features was generated.

To characterize these bilayered scaffolds, we evaluated quantitatively and qualitatively the extent of nanofiber deposition on top of a microfiber layer as a function of the duration of electrospinning time (Figures 6 and 7). Electrospinning for longer periods increased the amount of fiber deposition and, thereby, the thickness of the nanofiber layer. A quantitative analysis showing the percent of nanofiber coverage as a function of electrospinning time (15, 30, 60, and 90 s) is shown in Figure 6. At the shortest nanofiber electrospin time of 15 s, the nanofiber coverage varied from 1% to 40% with the majority of points examined displaying approximately 20% nanofiber coverage (Figure 7A); at a longer nanofiber electrospin time of 90 s, the coverage varied from 30% to 80% with the majority of points at approximately 60% nanofiber coverage (Figure 7D). After 120 s of electrospinning, the nanofiber layer appeared to cover the microfiber layer; the accumulation of the nanofiber layer after 300 s of electrospinning made it difficult to visually discern the microfibers underneath (Figure 7F). To further illustrate the versatility of the system, we electrospun a multilayered scaffold consisting of alternating layers of microfibers and nanofibers. Cross-sectional images of the layered scaffolds indicated that the layers produced by sequential electrospinning were well defined and distinguishable even when the nanofiber layer was thin (Figure 8).

The scaffold design presented herein integrates nanofibers and microfibers (both produced from electrospinning PCL) to form a single scaffold. As we have demonstrated, the thickness and coverage of the nanofiber layers can be controlled by modulating the electrospinning time of the nanofibers. Furthermore, the number, location, and spacing of the nanofiber layers could also be manipulated. Scaffolds containing different densities of nanofiber layers were used as model systems for investigating the cell infiltration into micro- and nanofiber scaffolds. Doing so provides critical information for the design of scaffolds to optimize the nanofiber (ECM scale mimic) and microfiber (allows for cell infiltration) balance.

Cellular Attachment, Spreading, and Infiltration. As a preliminary investigation into the potential application of the layered scaffolds, we evaluated cell attachment on 0, 30, 90, and 300 s scaffolds (Figures 3D, 7B, 7D, and 7F, respectively) at 2 and 24 h post-seeding. For all groups, more cells were attached at the 2 h time point than at 24 h; there were also significantly more cells attached on the 0 s scaffolds as compared to all other groups. After 24 h, however, the number

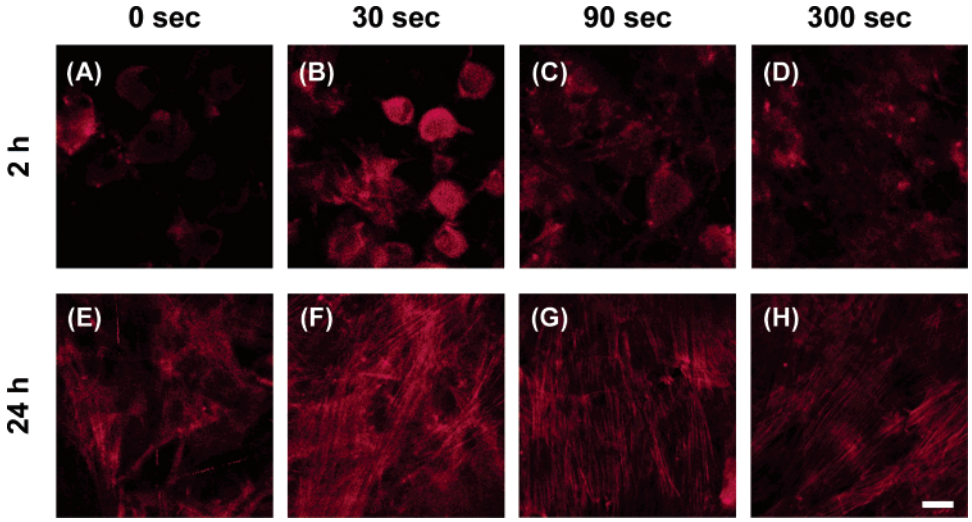

Figure 10. Laser scanning confocal microscope images of cells stained for F-actin with rhodamine phallodin at the top surface of 0 (A and E), 30 (B and F), 90 (C and G), and 300 s scaffolds (D and H) at 2 and 24 h (A−D and E−H, respectively). The 0, 30, 90, and 300 s scaffolds are bilayered scaffolds consisting of a bottom microfiber layer (5 μm) and a top nanofiber layer (600 nm); the numbers correspond to the time used to spin the nanofiber layer. The scale bar shown is 20 μm and applies to all images.

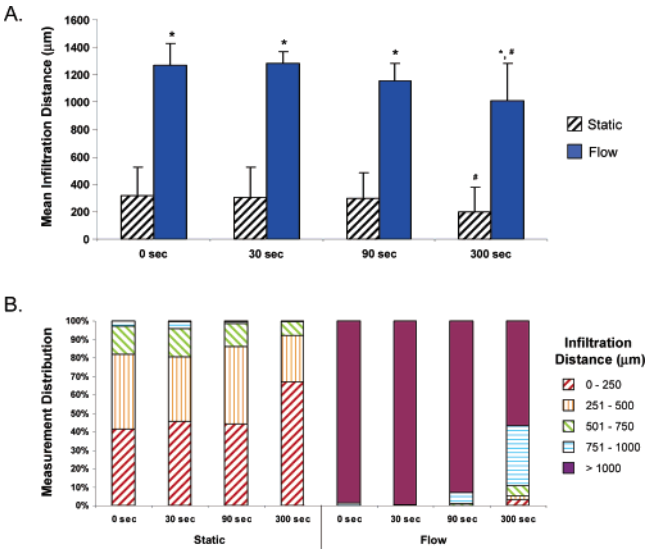

Figure 11. (A) Mean infiltration distance traversed by cells on 0, 30, 90, and 300 s scaffolds under static and flow culture conditions. The 0, 30, 90, and 300 s scaffolds are bilayered scaffolds consisting of a bottom microfiber layer (5 μm) and a top nanofiber layer (600 nm); the numbers correspond to the time used to spin the nanofiber layer. The data represent means of four samples, with error bars representing the standard deviations. A "*" indicates statistical significance between static and flow for each group; a "#" indicates that for that culture condition, a statistical significance exists between the 300 s group as compared to the other groups ($p < 0.01$). (B) Distribution of the measured infiltration distances separated into bins of 250 μm distances.

of cells attached on the scaffolds was statistically similar between groups, with approximately 40% attachment (Figure 9).

While cell attachment did not seem to be enhanced by nanofibers, cell spreading appeared to be affected (Figure 10). A distinct visual difference in actin staining could be observed between the 0 s and other groups. At 2 h, cells on the 0 s scaffold appeared round, while cells on 30, 90, and 300 s were more spread. At 24 h, cells on the 0 s scaffold became more spread and some actin filaments could be visualized; in contrast, the number of filaments observed at 24 h was greater on 30, 90, and 300 s scaffolds. Fiber diameter has been shown to affect the phenotypic expression of cells;[17,29,35] therefore, it is expected that the extent of spreading will play a role in the proliferation and differentiation of MSCs.

Figure 11 shows the mean infiltration measurements of cells on 0, 30, 90, and 300 s scaffolds along with distribution in infiltration measurements. Culturing the constructs in a flow perfusion bioreactor significantly enhanced the infiltration distance of MSCs by a factor of 5. Previous studies have also demonstrated that flow perfusion culture increases the distribution of cells as compared to static culture.[18,19] Flow perfusion culture is beneficial for mitigating mass transport limitations inherent in static culture.[46]

Complete infiltration (i.e., cells on both the top and the bottom of the scaffold) was only observed for constructs cultured in the bioreactor, illustrating the benefits of flow perfusion culture on the distribution of cells throughout 3D scaffolds (Figure 12). The effect of the nanofiber layer thickness on MSC infiltration is reflected in the infiltration measurements, where the presence of a 300 s nanofiber layer resulted in a significant decrease in infiltration distance as compared to the other scaffolds. This result indicates that increasing the thickness of the nanofiber layer can reduce the ability of MSCs to infiltrate through the scaffold porosity for the specific perfusion condition tested herein. Similar observations were made in static culture, in which the presence of a 300 s nanofiber layer also significantly reduced the infiltration distance of cells as compared to the other groups within the static culture condition, with maximum infiltration distances of only approximately 200 μm.

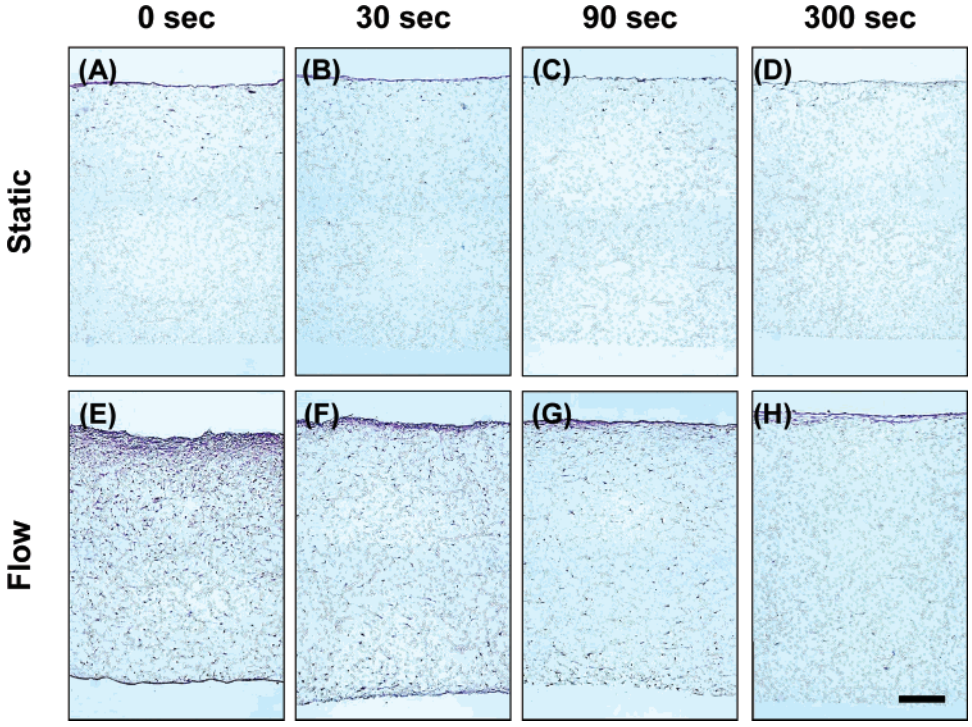

Figure 12. Light microscope images (10×) of histological sections stained with hematoxylin and eosin. (A−D) represents sections from 0, 30, 90, and 300 s scaffolds, respectively, cultured under static conditions. (E−H) represents sections from 0, 30, 90, and 300 s scaffolds, respectively, cultured under flow perfusion conditions. The 0, 30, 90, and 300 s scaffolds are bilayered scaffolds consisting of a bottom microfiber layer (5 μm) and a top nanofiber layer (600 nm); the numbers correspond to the time used to spin the nanofiber layer. The scale bar shown is 200 μm and applies to all images shown.

Taken together, these results provide insight into the use of nanofibers for tissue engineering applications. The data suggest that the incorporation of a dense nanofiber layer can hinder cell migration, presumably due to the smaller pore sizes. Contrarily, the inclusion of nanofibers influences cell spreading, which can play a role in the proliferation and differentiation of MSCs. As several studies have shown, cells are able to proliferate, differentiate, and maintain their phenotypic expression on nanofiber scaffolds.[27,36] Further studies are required to elucidate the effect of the inclusion of nanofibers on MSC function (e.g., proliferation, spreading, and differentiation) under conditions of static and flow culture.

Various methods have been undertaken to address the concern of poor cell migration into nanofiber scaffolds. One approach is to introduce micro-voids into the scaffold after spinning. A dual-porosity structure was created using a salt leaching/gas forming method in conjunction with electrospinning. However, the fiber morphology of the scaffolds appeared to be significantly affected by the post-spinning processes.[47] Alternatively, two different polymer solutions can be co-electrospun with one polymer acting as a leaching polymer to form micropores.[45] Zhang et al. reported improved migration when using a PCL/gelatin nanofiber composite scaffold after the gelatin fibers were leached; overall migration was approximately 115 μm in leached scaffolds as compared to 50 μm in plain PCL nanofiber scaffolds after 1 week of static culture.[34] In another strategy, a cellular solution was electrosprayed concomitantly with electrospinning of poly(ester urethane) urea such that cells became interspersed within the scaffold.[48] The setup, however, is considerably more complex than traditional electrospinning systems. Our strategy is to use microfiber scaffolds to generate the larger pore sizes while interspersing nanofiber layers throughout the construct to influence cell function.

Conclusion

The approach taken in this study was to exploit the extensive range of fiber diameters capable of being produced by electrospinning to generate scaffolds with unique properties. We demonstrated the ability to fabricate 3D microfiber scaffolds with controlled fiber diameters up to 10 μm. The average pore size of microfiber scaffolds was dependent on its fiber diameter and ranged from 10 to 45 μm, while the porosities were constant between 84% and 89%. To capitalize on the properties of both microfibers (i.e., pores large enough for cell migration) and nanofibers (i.e., physical mimicry of native ECM), multilayered scaffolds were fabricated. MSCs attached well on both single and bilayered scaffolds but were more spread when nanofibers were present. However, scaffolds with a 300 s nanofiber layer exhibited reduced cellular infiltration under both static and flow culture conditions tested herein. The optimization of the balance of nanofibers and microfibers in these multilayer structures could have tremendous potential for 3D tissue engineering applications.

Acknowledgment. This work was supported by a grant from the National Institutes of Health (R01-AR42639) (A.G.M.). U.S. acknowledges support from a training fellowship from the Keck Center Nanobiology Training Program of the Gulf Coast Consortia (NIH Grant No. 1 T90 DK070121-01).

References and Notes

(1) Lu, L.; Mikos, A. G. *MRS Bull.* **1996**, *21*, 28.
(2) Hutmacher, D. W. *Biomaterials* **2000**, *21*, 2529.
(3) Liu, X.; Ma, P. X. *Ann. Biomed. Eng.* **2004**, *32*, 477.
(4) Fisher, J. P.; Holland, T. A.; Dean, D.; Engel, P. S.; Mikos, A. G. *J. Biomater. Sci., Polym. Ed.* **2001**, *12*, 673.
(5) Lu, L.; Peter, S. J.; Lyman, M. D.; Lai, H. L.; Leite, S. M.; Tamada, J. A.; Uyama, S.; Vacanti, J. P.; Langer, R.; Mikos, A. G. *Biomaterials* **2000**, *21*, 1837.
(6) Lu, L.; Peter, S. J.; Lyman, M. D.; Lai, H. L.; Leite, S. M.; Tamada, J. A.; Vacanti, J. P.; Langer, R.; Mikos, A. G. *Biomaterials* **2000**, *21*, 1595.
(7) Cooke, M. N.; Fisher, J. P.; Dean, D.; Rimnac, C.; Mikos, A. G. *J. Biomed. Mater. Res. B* **2003**, *64*, 65.
(8) Wnek, G. E.; Carr, M. E.; Simpson, D. G.; Bowlin, G. L. *Nano Lett.* **2003**, *3*, 213.
(9) Subbiah, T.; Bhat, G. S.; Tock, R. W.; Pararneswaran, S.; Ramkumar, S. S. *J. Appl. Polym. Sci.* **2005**, *96*, 557.
(10) Deitzel, J. M.; Kleinmeyer, J.; Harris, D.; Tan, N. C. B. *Polymer* **2001**, *42*, 261.
(11) Fridrikh, S. V.; Yu, J. H.; Brenner, M. P.; Rutledge, G. C. *Phys. Rev. Lett.* **2003**, *90*, 144502.
(12) Pham, Q. P.; Sharma, U.; Mikos, A. G. *Tissue Eng.* **2006**, *12*, 1197.
(13) Datta, N.; Pham, Q. P.; Sharma, U.; Sikavitsas, V. I.; Jansen, J. A.; Mikos, A. G. *Proc. Natl. Acad. Sci. U.S.A.* **2006**, *103*, 2488.
(14) Eichhorn, S. J.; Sampson, W. W. *J. R. Soc. Int.* **2005**, *2*, 309.
(15) Goldstein, A. S.; Zhu, G.; Morris, G. E.; Meszlenyi, R. K.; Mikos, A. G. *Tissue Eng.* **1999**, *5*, 421.
(16) Karageorgiou, V.; Kaplan, D. *Biomaterials* **2005**, *26*, 5474.
(17) Holtorf, H. L.; Datta, N.; Jansen, J. A.; Mikos, A. G. *J. Biomed. Mater. Res. A* **2005**, *74*, 171.
(18) Sikavitsas, V. I.; Bancroft, G. N.; Lemoine, J. J.; Liebschner, M. A.; Dauner, M.; Mikos, A. G. *Ann. Biomed. Eng.* **2005**, *33*, 63.
(19) Gomes, M. E.; Sikavitsas, V. I.; Behravesh, E.; Reis, R. L.; Mikos, A. G. *J. Biomed. Mater. Res. A* **2003**, *67*, 87.
(20) Flemming, R. G.; Murphy, C. J.; Abrams, G. A.; Goodman, S. L.; Nealey, P. F. *Biomaterials* **1999**, *20*, 573.
(21) Yang, S. F.; Leong, K. F.; Du, Z. H.; Chua, C. K. *Tissue Eng.* **2001**, *7*, 679.
(22) Woodfield, T. B.; Van Blitterswijk, C. A.; De Wijn, J.; Sims, T. J.; Hollander, A. P.; Riesle, J. *Tissue Eng.* **2005**, *11*, 1297.
(23) Schwarz, K.; Epple, M. *Macromol. Rapid Commun.* **1998**, *19*, 613.
(24) Li, W. J.; Laurencin, C. T.; Caterson, E. J.; Tuan, R. S.; Ko, F. K. *J. Biomed. Mater. Res. A* **2002**, *60*, 613.
(25) Schindler, M.; Ahmed, I.; Kamal, J.; Nur, E. K. A.; Grafe, T. H.; Young Chung, H.; Meiners, S. *Biomaterials* **2005**, *26*, 5624.
(26) Boland, E. D.; Matthews, J. A.; Pawlowski, K. J.; Simpson, D. G.; Wnek, G. E.; Bowlin, G. L. *Front. Biosci.* **2004**, *9*, 1422.
(27) Kwon, I. K.; Kidoaki, S.; Matsuda, T. *Biomaterials* **2005**, *26*, 3929.
(28) Min, B. M.; Lee, G.; Kim, S. H.; Nam, Y. S.; Lee, T. S.; Park, W. H. *Biomaterials* **2004**, *25*, 1289.
(29) Badami, A. S.; Kreke, M. R.; Thompson, M. S.; Riffle, J. S.; Goldstein, A. S. *Biomaterials* **2006**, *27*, 596.
(30) Matthews, J. A.; Wnek, G. E.; Simpson, D. G.; Bowlin, G. L. *Biomacromolecules* **2002**, *3*, 232.
(31) Yoshimoto, H.; Shin, Y. M.; Terai, H.; Vacanti, J. P. *Biomaterials* **2003**, *24*, 2077.
(32) Tuzlakoglu, K.; Bolgen, N.; Salgado, A. J.; Gomes, M. E.; Piskin, E.; Reis, R. L. *J. Mater. Sci.: Mater. Med.* **2005**, *16*, 1099.
(33) Mo, X. M.; Xu, C. Y.; Kotaki, M.; Ramakrishna, S. *Biomaterials* **2004**, *25*, 1883.
(34) Zhang, Y.; Ouyang, H.; Lim, C. T.; Ramakrishna, S.; Huang, Z. M. *J. Biomed. Mater. Res. B* **2005**, *72*, 156.
(35) Takahashi, Y.; Tabata, Y. *J. Biomater. Sci., Polym. Ed.* **2004**, *15*, 41.
(36) Li, W. J.; Tuli, R.; Huang, X.; Laquerriere, P.; Tuan, R. S. *Biomaterials* **2005**, *26*, 5158.
(37) Grant, P. V.; Vaz, C. M.; Tomlins, P. E.; Mikhalovska, L.; James, S.; Mikhalovsky, S.; Vadgama, P. *Physical Characterization of a Polycaprolactone Tissue Scaffold*; National Physical Laboratory: Teddington, United Kingdom, 2005.
(38) Hu, Y.; Grainger, D. W.; Winn, S. R.; Hollinger, J. O. *J. Biomed. Mater. Res. A* **2002**, *59*, 563.
(39) Holy, C. E.; Yakubovich, R. *J. Biomed. Mater. Res. A* **2000**, *50*, 276.
(40) Jaeger, R.; Bergshoef, M. M.; Batlle, C. M. I.; Holger, S.; Vansco, G. J. *Macromol. Symp.* **1998**, *127*, 141.
(41) Venugopal, J.; Ramakrishna, S. *Tissue Eng.* **2005**, *11*, 847.
(42) Mikos, A. G.; Thorsen, A. J.; Czerwonka, L. A.; Bao, Y.; Langer, R.; Winslow, D. N.; Vacanti, J. P. *Polymer* **1994**, *35*, 1068.
(43) Ho, S. T.; Hutmacher, D. W. *Biomaterials* **2006**, *27*, 1362.
(44) Sampson, W. W. *J. Mater. Sci.* **2003**, *38*, 1617.
(45) Kidoaki, S.; Kwon, I. K.; Matsuda, T. *Biomaterials* **2005**, *26*, 37.

(46) Goldstein, A. S.; Juarez, T. M.; Helmke, C. D.; Gustin, M. C.; Mikos, A. G. *Biomaterials* **2001**, *22*, 1279.
(47) Lee, Y. H.; Lee, J. H.; An, I. G.; Kim, C.; Lee, D. S.; Lee, Y. K.; Nam, J. D. *Biomaterials* **2005**, *26*, 3165.
(48) Stankus, J. J.; Guan, J.; Fujimoto, K.; Wagner, W. R. *Biomaterials* **2006**, *27*, 735.

BM060680J